Journal for ImmunoTherapy of Cancer

Blockade of CLEVER-1 restrains immune evasion and enhances anti-PD-1 immunotherapy in gastric cancer

Kuan Yu ,[1,2] Yifan Cao,[1,2] Zihao Zhang,[1,2] Leihao Wang,[1,2] Yichao Gu,[1,2] Tianwei Xu,[1] Xiaolei Zhang,[3] Xinxin Guo,[3] Zhenbin Shen,[1,2] Jing Qin [1,2]

To cite: Yu K, Cao Y, Zhang Z, *et al*. Blockade of CLEVER-1 restrains immune evasion and enhances anti-PD-1 immunotherapy in gastric cancer. *Journal for ImmunoTherapy of Cancer* 2025;**13**:e011080. doi:10.1136/jitc-2024-011080

► Additional supplemental material is published online only. To view, please visit the journal online (https://doi.org/10.1136/jitc-2024-011080).

KY, YC and ZZ contributed equally.

Accepted 16 April 2025

[1]Department of General Surgery, Zhongshan Hospital Fudan University, Shanghai, China
[2]Gastric Cancer Center, Zhongshan Hospital Fudan University, Shanghai, China
[3]Department of Pathology, Zhongshan Hospital Fudan University, Shanghai, China

Correspondence to
Dr Jing Qin;
qin.jing@zs-hospital.sh.cn

Dr Zhenbin Shen;
shen.zhenbin@zs-hospital.sh.cn

ABSTRACT

Background Gastric cancer (GC) remains a major global health burden. Despite the advancements in immunotherapy for patients with GC, the heterogeneity of GC limits response rates, especially in immune "cold" subtypes, including genomically stable and epithelial-mesenchymal transition GC. Common lymphatic endothelial and vascular endothelial receptor-1 (CLEVER-1), a newly recognized immune checkpoint molecule predominantly expressed on tumor-associated macrophages (TAMs), remains poorly understood in GC. This study aims to explore the clinical significance of CLEVER-1$^+$TAM infiltration, elucidate its role in modulating the tumor immune landscape, and investigate the therapeutic potential of CLEVER-1 blockade in enhancing immunotherapy.

Methods This study analyzed two independent GC cohorts and single-cell RNA sequencing data (GSE183904). CLEVER-1 expression in TAMs was assessed via multiplex immunofluorescence, flow cytometry, and RNA sequencing. The clinical relevance of CLEVER-1$^+$TAM infiltration was evaluated in relation to tumor, node, metastases staging, molecular subtypes, prognosis, and immunochemotherapy response. Transcriptomic and pathway analyses characterized the immunophenotype of CLEVER-1$^+$TAMs. Functional assays examined their suppression on CD8$^+$T cells, while interventional experiments assessed the impact of CLEVER-1 blockade alone or with programmed cell death protein-1 (PD-1) inhibition.

Results CLEVER-1 was predominantly expressed on TAMs in GC and was associated with worse clinical outcomes. Transcriptomic and phenotypic analyses revealed that CLEVER-1$^+$TAMs display a dynamic immunophenotype and critically suppress T-cell function, fostering an immunosuppressive microenvironment. High CLEVER-1$^+$TAM infiltration was linked to poor response or adaptive resistance to PD-1 blockade therapy. CLEVER-1 blockade reprogrammed TAMs toward a pro-inflammatory phenotype, resulting in enhanced CD8$^+$T cell cytotoxicity and proliferation. Co-targeting CLEVER-1 and PD-1 synergistically enhanced antitumor responses.

Conclusions High infiltration of CLEVER-1$^+$TAMs indicates immune suppression and poor prognosis in GC. The combination of CLEVER-1 and PD-1 blockade emerges as a dual-pronged strategy to boost immune-mediated tumor control and prevent treatment relapse in GC.

WHAT IS ALREADY KNOWN ON THIS TOPIC

⇒ Gastric cancer (GC)'s immunotherapy puzzle book lies open, its crucial chapters awaiting ink. Common lymphatic endothelial and vascular endothelial receptor-1 (CLEVER-1) is an emerging, targetable immune checkpoint molecule primarily expressed on tumor-associated macrophages (TAMs), but its role in GC remains unclear.

WHAT THIS STUDY ADDS

⇒ CLEVER-1$^+$TAMs in GC exhibit a mixed immune phenotype, which gradually polarizes toward an immunosuppressive state as the tumor progresses.

⇒ CLEVER-1$^+$TAMs impair the efficacy of programmed cell death protein-1 (PD-1) inhibitors and are associated with immune therapy resistance.

⇒ CLEVER-1 blockade combined with PD-1 inhibitors significantly enhances CD8$^+$T cell-mediated antitumor effects.

HOW THIS STUDY MIGHT AFFECT RESEARCH, PRACTICE OR POLICY

⇒ CLEVER-1$^+$TAMs may become a novel biomarker for predicting patients with GC who could benefit from anti-PD-1 therapy and highlights them as a promising target for overcoming immunotherapy resistance in GC.

INTRODUCTION

Gastric cancer (GC), a highly prevalent and deadly malignancy, remains a major global health concern, particularly in eastern and southeastern Asia.[1 2] It ranks as the fifth most common cancer worldwide, with approximately 1 million new cases diagnosed each year.[3] Due to its often asymptomatic in its early stages, GC is frequently diagnosed at advanced stages.[4 5] This contributes to its ranking as the fourth leading cause of cancer-related deaths.[6] Despite notable advancements in therapeutic strategies, the pace of clinical progress in GC remains incremental. Apart from radical resection, which remains the only potentially curative intervention, chemotherapy continues to

be an irreplaceable cornerstone in the management of advanced-stage disease.[5] Despite its recent regulatory approval and enthusiasm in academia, immunotherapy remains limited by modest response rates, diminishing its therapeutic value as a standalone treatment in GC.[7] Consequently, immunotherapy is currently administered alongside chemotherapy in clinical practice,[8] a strategy that plays to its inherent strengths while mitigating its limitations. In light of these challenges, understanding the composition and interactions of immune cells within tumors becomes critical for developing more effective treatment strategies. Therefore, there is an urgent need to identify strategies that enhance the efficacy of immunotherapy and even potentially replace chemotherapy in specific subsets of patients with GC, thereby achieving enhanced therapeutic efficacy with reduced chemotherapy-induced toxicities.

Immunotherapy and chemotherapy differ in that chemotherapy non-specifically targets rapidly dividing cancer cells, whereas immunotherapy enhances the immune system's ability to identify and attack tumor cells specifically.[9] Understanding these differences, especially within the context of the tumor microenvironment (TME), is vital for developing new treatment approaches. The complex interactions of immune cells in the TME often hinder T cell-centric immunotherapy strategies,[10 11] highlighting the need for a more systematic approach to enhance efficacy. The TME is marked by chronic inflammation, leading some to describe tumors as "wounds that do not heal".[12] Myeloid cells, particularly tumor-associated macrophages (TAMs), play a pivotal role in remodeling the immune microenvironment.[13] TAMs exhibit remarkable plasticity, allowing them to adapt their functions based on various factors within the TME and polarize into different phenotypes.[14] Traditionally, macrophages are recognized for acquiring either antitumor M1 or pro-tumor M2 functional phenotypes.[15] However, recent studies indicate that TAMs encompass various functional subpopulations that contribute to immune regulation.[16–18]

Common lymphatic endothelial and vascular endothelial receptor-1 (CLEVER-1), also referred to as Stabilin-1 or Feel-1, is a versatile adhesion and scavenger receptor that is produced by the *STAB1* gene.[19] It is present in specific types of endothelial cells and TAMs.[20] While its role as an adhesion and scavenger receptor has been well documented,[21 22] its emerging functions in innate-adaptive immune crosstalk and cancer-related immune regulation are gaining interest.[23] Recent studies have identified CLEVER-1 as a promising target for cancer immunotherapy.[24 25] Early-phase clinical research has pioneered the exploration of CLEVER-1 as a therapeutic target in patients with advanced solid tumors (NCT03733990).[26] However, the distribution of CLEVER-1 in GC and its involvement in tumor progression, along with the feasibility and mechanisms of CLEVER-1-targeted interventions in this context, remain largely undefined and require further investigation. To address these gaps, our study systematically examines CLEVER-1 in GC, elucidating its potential impact on immune modulation and disease advancement and exploring its value in optimizing therapeutic strategies.

MATERIALS AND METHODS

Patients and specimens

The study involved two separate cohorts of patients with GC from our center. The Zhongshan Cohort (n=135) underwent radical D2 gastrectomy between March 2010 and August 2012 (follow-up until August 2022). The Zhongshan Flow Cytometry (ZSFC) Cohort (n=60) underwent D2 gastrectomy between September 2018 and July 2019 (follow-up until January 2024). Tumor stages were determined according to the eighth edition of the American Joint Committee on Cancer Staging System, and overall survival (OS) and disease-free survival (DFS) were the primary outcomes. (Clinicopathological details stratified by CLEVER-1$^+$TAM infiltration are provided in online supplemental table S1).

Additionally, single-cell RNA sequencing (scRNA-seq) data from 26 primary gastric tumors (GEO: GSE183904[27]) reported by Kumar *et al*[28] were analyzed. 72 fresh tumor samples were collected for specific experimental analyses between June 2023 and February 2025.

To investigate the correlation between CLEVER-1$^+$TAM infiltration and response to anti-programmed cell death protein-1 (PD-1) therapy, 12 patients with GC who underwent curative resection following four cycles of SOX (S-1 plus oxaliplatin) + PD-1 inhibitor immunochemotherapy were enrolled (March 2023 to June 2024) at our center. Pretreatment endoscopic biopsy specimens and paired post-treatment surgical tissues were collected and stratified by the JGCA histological response grading system[29] (Grade 1: non-responders, Grades 2 and 3: responders).

Detailed sample information and allocation are provided in online supplemental materials and online supplemental table S2

Multiplex immunofluorescence and IHC SCORE quantification

Multiplex immunofluorescence was performed on formalin-fixed, paraffin-embedded (FFPE) tumor microarrays (TMAs) following standard protocols. After antigen retrieval and blocking, slides were incubated with primary antibodies overnight at 4°C, followed by horseradish peroxidase-conjugated secondary antibodies and tyramide signal amplification (TSA) fluorescence development. Staining was repeated for multiplex labeling, and slides were counterstained with 4',6-diamidino-2-phenylindole. Detailed staining procedures are provided in online supplemental material 2.

Two independent pathologists evaluated CLEVER-1$^+$TAM and CD8$^+$T cell infiltration in three representative high-power fields (HPFs, ×40 magnification) per sample. Images were acquired using CaseViewer V.2.4.0 (3DHISTECH, Hungary), and evaluations were performed blindly to clinical data. The final immunohistochemistry (IHC) score was calculated as (mean CLEVER-1$^+$TAM

count per HPF)×4, with patients stratified into high-infiltration and low-infiltration groups based on the median cut-off. Detailed scoring criteria and evaluation methods are provided in online supplemental method 3.

Flow cytometry

Fresh tumor tissues were enzymatically digested to obtain single-cell suspensions, followed by GolgiStop (BD Biosciences, Franklin Lakes, New Jersey, USA) treatment, and red blood cell lysis Cells (BD Biosciences) were stained with FVS510 (BD Biosciences) for viability assessment, followed by Fc receptor blocking (BD Biosciences) and surface marker staining. For intracellular staining, cells were fixed, permeabilized, and incubated with specific antibodies. Flow cytometry (FCM) and intracellular flow cytometry were performed using an FACSAria III (BD Biosciences), and data were analyzed with FlowJo software (TreeStar, San Carlos, California, USA). Detailed staining protocols and reagent information are provided in online supplemental methods 4 and 5.

Magnetic-activated cell sorting and RNA sequencing

Single-cell suspensions from eight freshly resected GC tissues were incubated with either IgG_4 (control, 25 µg/mL, BioLegend) or CLEVER-1 blockade (bexmarilimab, antibody, 25 µg/mL, MedChemExpress) in Roswell Park Memorial Institute (RPMI) 1640 with 10% fetal bovine serum (FBS and 1% penicillin-streptomycin (Gibco) at 37°C, 5% CO_2 for 12 hours. TAMs were then isolated using a human CD14 selection kit (MojoSort, BioLegend) and immediately lysed (10x Genomics) for RNA extraction (figure 1A). Complementary DNA libraries were generated using Smart-seq2, and RNA sequencing was performed on the NovaSeq 6000 (Illumina). Reads were aligned to the human transcriptome using HISAT2, and differentially expressed genes (DEGs) were identified using DESeq2 (V.1.34.0) in R (V.4.3.1). Functional annotation was conducted via Gene Ontology (GO) analysis (DAVID, https://david.ncifcrf.gov/tools.jsp) and Gene Set Enrichment Analysis.

Ex vivo tumor inhibition assay

Single-cell suspensions derived from 28 freshly resected GC tissues were divided into four treatment groups (figure 2A): isotype control (IgG4, 25 µg/mL); CLEVER-1 blockade (bexmarilimab, 25 µg/mL); nivolumab (anti-PD-1 antibody, 25 µg/mL, MedChemExpress); and combined blockade subgroup (bexmarilimab+nivolumab, 25 µg/mL each). Cells were cultured in RPMI 1640 with 10% FBS and 1% penicillin-streptomycin at 37°C and 5% CO_2 for 12 hours.

After incubation, cells were harvested for analysis. $CD8^+$T cell phenotyping was performed using FCM, and tumor cell apoptosis was assessed using Annexin V/PI staining following the manufacturer's protocol (BD Biosciences). Stained cells were analyzed by FCM to quantify apoptotic and necrotic cell populations.

In vitro TAM/$CD8^+$T cell co-culture system

Ficoll (Cytiva, GE Life) was used to isolate human peripheral blood mononuclear cells (PBMCs), and $CD8^+$T cells were purified using human CD8 nanobeads (MojoSort, BioLegend). For the co-culture assay, bead-purified peripheral CD8 T cells (1×10^5 cells per well in 24-well plates) were initially activated for 3 days in RPMI 1640 complete medium, recombinant human interleukin (IL)-2 (60 ng/mL, BioLegend), anti-CD3 (10 µg/mL, Cell Signaling Technology), and anti-CD28 (2 µg/mL, Cell Signaling Technology) (see online supplemental figure 5A). After this activation period, the cells were divided into three groups cultured for an additional 36 hours: one group continued to be cultured as activated $CD8^+$T cells alone, while the other two groups were co-cultured with TAMs isolated from tumor tissues that had been pretreated with isotype control (IgG4, 25 µg/mL) or CLEVER-1 blockade (bexmarilimab, 25 µg/mL), as described previously. After 36 hours, $CD8^+$T cells were harvested for proliferation, apoptosis, and functional assays.

Statistical analysis

Continuous variables were assessed for normality using the Shapiro-Wilk test. Data are expressed as mean (±SD) for normally distributed variables and as median (±IQR) for non-normally distributed variables. For two-group comparisons, unpaired t-tests were used for normally distributed data and one-way analysis of variance with Tukey's post hoc test was applied for multigroup comparisons. For non-normally distributed data, the Wilcoxon or Mann-Whitney U test was used for two groups, and the Kruskal-Wallis test with Dunn's post hoc test was applied for multigroup analyses. Categorical variables were compared using the χ^2 test. Survival analyses employed Kaplan-Meier curves and the log-rank test, while multivariate analyses used the Cox proportional hazards model to derive HRs and 95% CIs and to evaluate covariate effects.

Statistical analyses were performed using IBM SPSS Statistics V.25.0, MedCalc V.15.6.1, GraphPad Prism V.10.2.1, and R V.4.3.1. A two-tailed p value<0.05 was considered statistically significant. Data visualizations were generated using GraphPad Prism V.10.2.1 and ggplot2 V.3.4.3 in R.

Additional methodological details can be found in the online supplemental materials; detailed information about the associated antibodies is provided in online supplemental table S3.

RESULTS

CLEVER-1 is predominantly expressed on tumor-associated macrophages in the tumor microenvironment of GC

To investigate the expression of CLEVER-1 in the TME of GC, we used Uniform Manifold Approximation and Projection (UMAP) analysis of scRNA-seq data from 26 primary gastric tumor tissue (GSE183904[27]). UMAP identified 12 distinct cell clusters, including T cells, natural

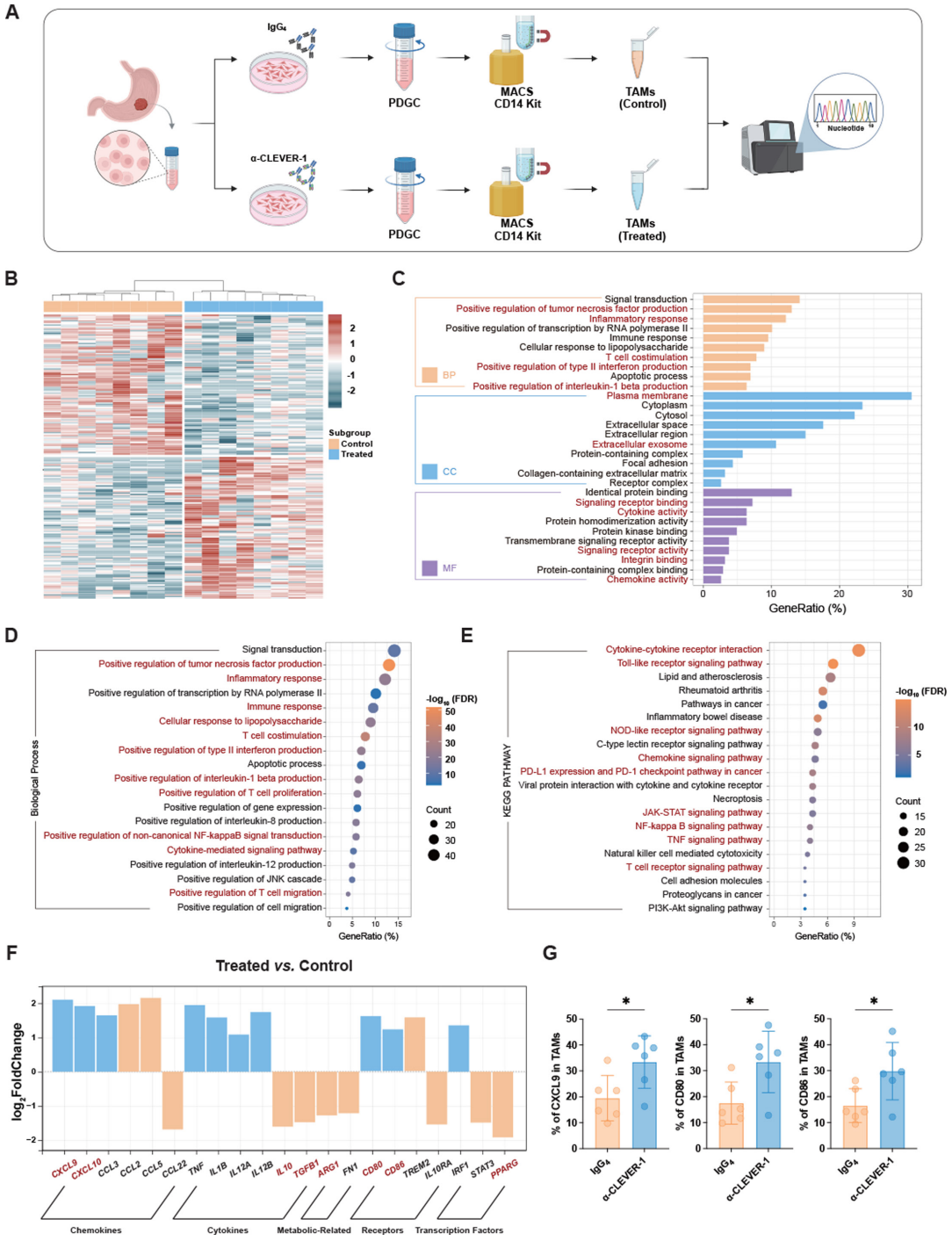

Figure 1 Target CLEVER-1 with a blocking antibody reshapes TAMs toward a pro-inflammatory phenotype in GC. (A) Schematic representation of the experimental design for CLEVER-1 blockade in TAMs (n=8). (B) Heatmap illustrating the expression patterns of DEGs in TAMs following anti-CLEVER-1 treatment compared with the IgG_4 control group. (C) GO enrichment analysis of upregulated DEGs in TAMs following CLEVER-1 blockade in GC highlighting key biological processes, cellular components, and molecular functions. (D–E) Dot plots illustrating significantly enriched GO biological processes (D) and Kyoto Encyclopedia of Genes and Genomes pathways (E) in TAMs following CLEVER-1 blockade. (F) Bar plot illustrating the differential expression of key chemokines, cytokines, metabolism-related genes, receptors, and transcription factors on CLEVER-1-blocked TAMs compared with the IgG_4 control. (G) Bar plots showing the expression of pro-inflammatory markers (CXCL9, CD80, and CD86) in TAMs following CLEVER-1 blockade or IgG_4 control by flow cytometry (n=6). Statistical analysis by two-tailed unpaired t-test. Small horizontal lines indicate the mean (±SD) *p<0.05 α-CLEVER-1, anti-CLEVER-1 antibody; CLEVER-1, common lymphatic endothelial and vascular endothelial receptor-1; DEG, differentially expressed gene; FN1, fibronectin 1; GO, Gene Ontology; IgG_4, immunoglobulin G4; IRF1, interferon regulatory factor 1; MACS, magnetic-activated cell sorting; PDGC, Percoll density gradient centrifugation; PPARG, peroxisome proliferator-activated receptor gamma; STAT3, signal transducer and activator of transcription 3; TAM, tumor-associated macrophage; TGFB1, transforming growth factor beta 1; TNF, tumor necrosis factor; TREM2, triggering receptor expressed on myeloid cells 2.

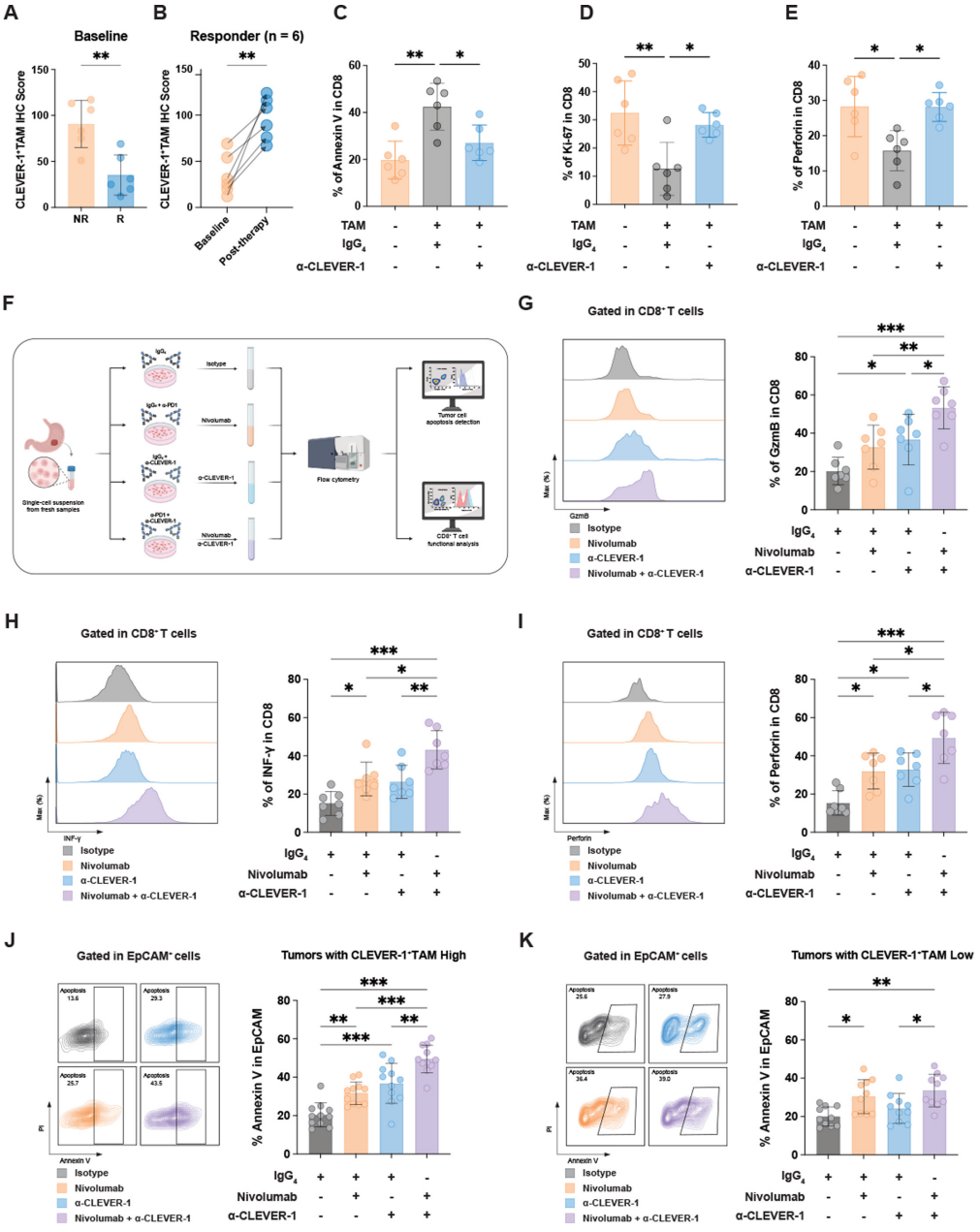

Figure 2 CLEVER-1 blockade synergizes with nivolumab to reinvigorate CD8$^+$ T-cell antitumor activity to reverse CLEVER-1$^+$ TAM-mediated immunosuppression in GC. (A) Bar plot comparing baseline CLEVER-1$^+$TAM infiltration between non-responders (NR, n=6) and responders (R, n=6) to immunochemotherapy. Statistical analysis by two-tailed unpaired t-test. Small horizontal lines indicate the mean (±SD). **p<0.01. (B) Paired analysis of CLEVER-1$^+$TAM Infiltration in responders at baseline and post-immunochemotherapy. Statistical analysis by two-tailed paired t-test. **p<0.01. (C–D) Bar plots showing the apoptotic rate (C), proliferative potential (D) and cytotoxic activity (E) of CD8$^+$T cells, as determined by FCM following co-culture with IgG_4-treated TAMs, α-CLEVER-1-treated TAMs, or in the absence of TAMs (n=6). Statistical analysis was conducted using ordinary one-way ANOVA followed by Tukey's multiple comparisons test. Small horizontal lines indicate the mean (±SD). *p<0.05, **p<0.01. (F) Schematic representation of the experimental design for the intervention with CLEVER-1 blockade, nivolumab, or their combination. (G–I) FCM analysis of effector cytokine expression, including GzmB (G), IFN-γ (H), and perforin (I), in CD8$^+$T cells across different treatment groups. Histogram overlays depict cytokine expression levels, while bar graphs quantify the percentage of GZMB$^+$, IFN-γ$^+$, and perforin$^+$CD8$^+$ T cells. Statistical analysis was conducted using ordinary one-way ANOVA followed by Tukey's multiple comparisons test. Small horizontal lines indicate the mean (±SD). *p<0.05, **p<0.01, ***p<0.001. (J–K) FCM analysis of apoptotic tumor cell frequency in CLEVER-1$^+$TAM high infiltration GC tissues (n=11, (J) and CLEVER-1$^+$TAM low infiltration GC tissues (n=10, (K). Statistical analysis was conducted using ordinary one-way ANOVA followed by Tukey's multiple comparisons test. Small horizontal lines indicate the mean (±SD). *p<0.05, **p<0.01, ***p<0.001. ACRG, Asian Cancer Research Group; ANOVA, analysis of variance; CIN, Chromosomal Instability; CLEVER-1, common lymphatic endothelial and vascular endothelial receptor-1; EBV, Epstein-Barr virus; EMT, epithelial-mesenchymal transition; FCM, flow cytometry; IFN, interferon; IHC, immunohistochemistry; GC, gastric cancer; GS, genomically stable; GzmB, granzyme B; MSI, microsatellite instability; MSS, microsatellite stable; TAM, tumor-associated macrophage; TCGA, The Cancer Genome Atlas.

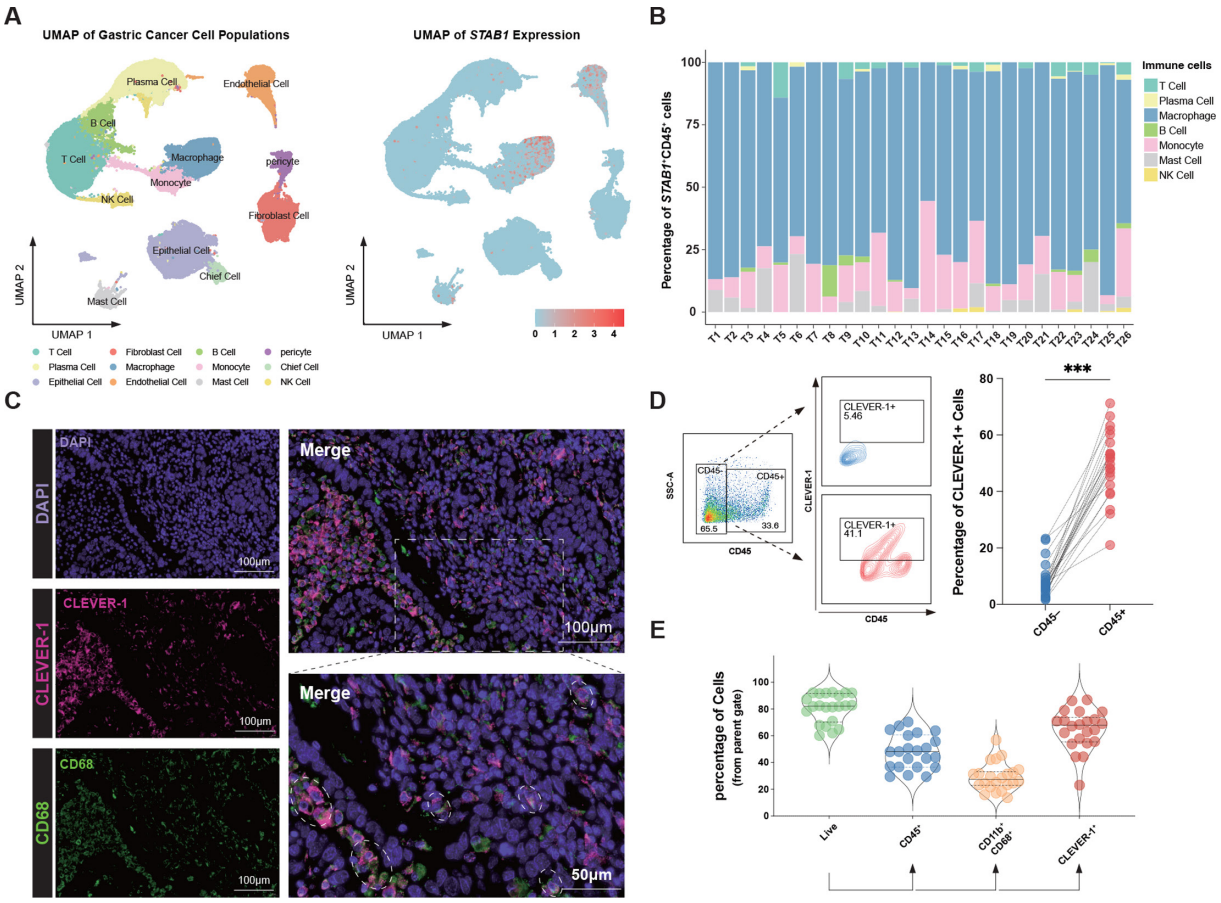

Figure 3 CLEVER-1 is predominantly expressed on TAMs in GC. (A) UMAP visualization of GC cell populations and CLEVER-1 (*STAB1*) expression illustrating 12 distinct clusters identified from scRNA-seq of 26 GC tumor tissues (left), with *STAB1* expression levels indicated by a gradient from light blue to dark red across these cell populations (right). (B) Stacked bar chart showing the distribution of *STAB1*$^{+}$CD45^{+} cell subsets across immune cell types in multiple patient samples. (C) Representative immunofluorescence images showing the expression of CLEVER-1 (magenta) and CD68 (green) in TME. Nuclei are counterstained with DAPI (blue). The rightmost panel shows merged images with two magnifications (scale bars: 100 μm and 50 μm). (D) Representative FCM plots demonstrating the different CLEVER-1 expression levels between CD45^{+} and CD45^{-} cells from GC tissues (left). A paired dot plot shows the quantitative data (right). Statistical analysis by two-tailed paired Wilcoxon test. ***p<0.001. (E) Violin plots illustrating the percentage distribution of live, CD45^{+}, CD11b^{+}CD68^{+}, and CLEVER-1^{+} cells from GC tissues (n=22), as determined by FCM analysis. CLEVER-1, common lymphatic endothelial and vascular endothelial receptor 1; DAPI, 4',6-diamidino-2-phenylindole; FCM, flow cytometry; GC, gastric cancer; HLA-DR, human leukocyte antigen-DR; IL, interleukin; NK, natural killer; scRNA-seq, single-cell RNA sequencing; TAM, tumor-associated macrophage; TGF, transforming growth factor; TME, tumor microenvironment; TNF, tumor necrosis factor; UMAP, Uniform Manifold Approximation and Projection.

killer cells, B cells, plasma cells, epithelial cells, fibroblasts, macrophages, endothelial cells, monocytes, mast cells, pericytes, and chief cells (figure 3A). Marker gene analysis confirmed the identity of these clusters (online supplemental figure 1A). Next, we visualize *STAB1* (encoding CLEVER-1) expression across these clusters. *STAB1* was predominantly expressed in macrophages and endothelial cells (figure 3A). To further characterize *STAB1*$^{+}$ immune cells, we quantified *STAB1*$^{+}$CD45^{+} cells within each immune subset (figure 3B). Macrophages (blue) exhibited the highest proportion of *STAB1*$^{+}$CD45^{+} cells, followed by monocytes (pink), suggesting that *STAB1* expression is predominantly expressed in TAMs.

Immunofluorescence staining of FFPE GC tissues, confirming the co-expression of CLEVER-1 and human TAM-specific marker CD68 (figure 3C). In addition, FCM analysis revealed significantly higher expression of CLEVER-1 in CD45^{+} cells compared with CD45^{-} cells (p<0.001, figure 3D). Furthermore, violin plots illustrate that CLEVER-1-expressing TAMs were abundant in GC tissue (figure 3E). Collectively, these findings highlight the substantial infiltration of CLEVER-1^{+}TAMs in the GC TME.

CLEVER-1^{+}TAM infiltration correlates with adverse clinicopathological characteristics and poor prognosis in GC

To evaluate the clinical significance of CLEVER-1^{+}TAMs in GC, we analyzed their association with TNM stage (figure 4A, online supplemental figure 2A). CLEVER-1^{+}TAM infiltration increased with advancing TNM stages, with significant differences observed between stages I and III (χ^2 test, p<0.001) and between stages II and III (χ^2 test,

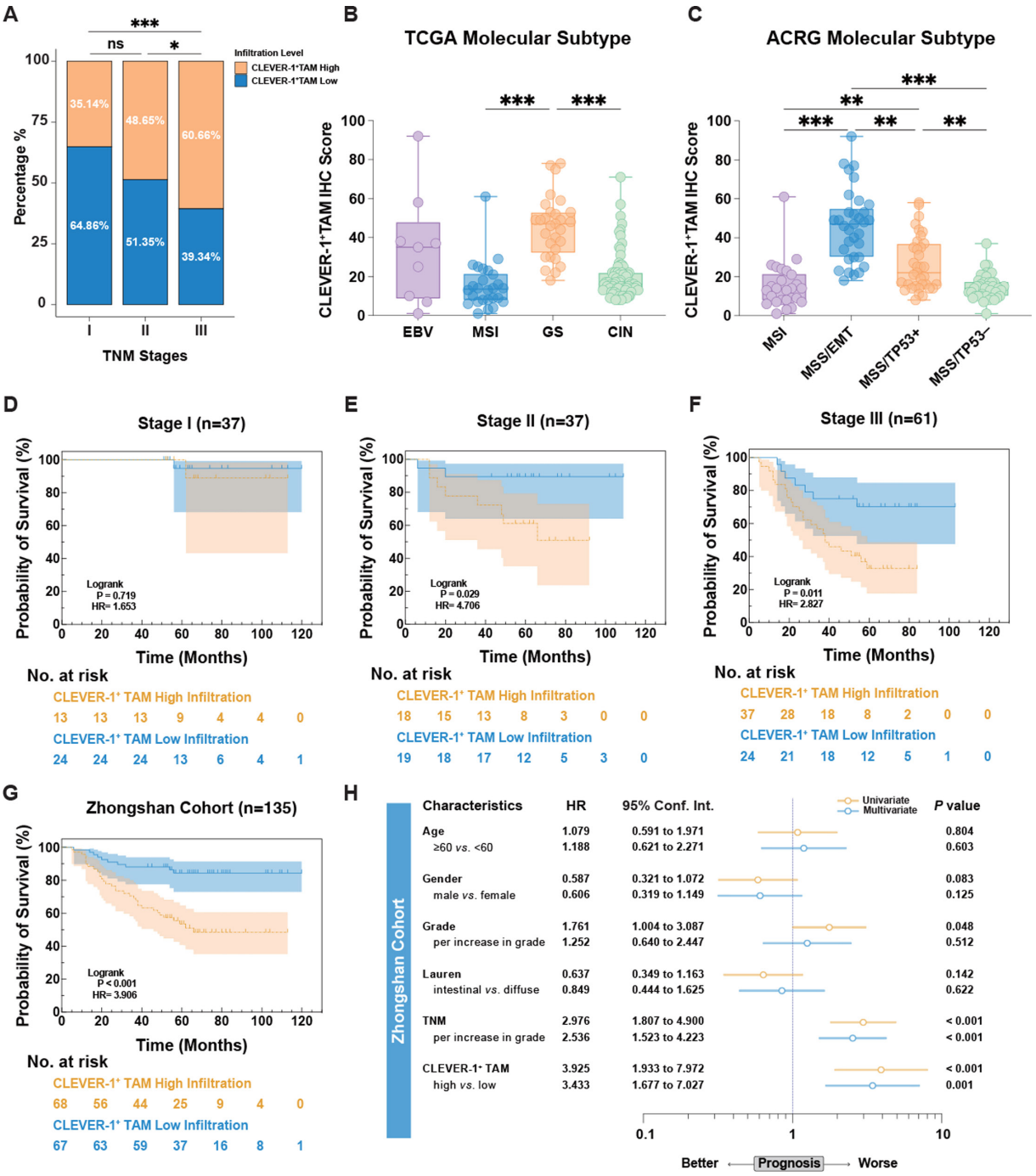

Figure 4 Clinical prognostic value of CLEVER-1$^+$TAMs in GC. (A) Stacked bar chart showing the distribution of CLEVER-1$^+$TAM infiltration across different tumor, node, metastases stages. Statistical analysis by χ^2 test. n.s: not significant, *p<0.05, **p<0.01, ***p<0.001. (B–C) Box-and-whiskers plots showing variations in CLEVER-1$^+$TAM infiltration among TCGA molecular subtypes (EBV, Epstein-Barr virus, MSI, GS, and CIN) (B) and ACRG molecular subtypes (MSI, MSS/epithelial-mesenchymal transition, MSS/TP53+, and MSS/TP53–) (C). Statistical analysis was performed using the Kruskal-Wallis test and Dunn's multiple comparisons tests. Box shows the median (±IQR), and whiskers indicate min-max values. *p<0.05, **p<0.01, ***p<0.001. (D–G) Kaplan-Meier survival curves for OS, stratified by CLEVER-1$^+$TAM infiltration levels in different patient groups from the Zhongshan Cohort: stage I (D), stage II (E), stage III (F), and all patients with GC (G). Statistical analysis was performed using the log-rank test, with survival probabilities shown as 95% CIs. (H) Forest plot displaying univariate and multivariate Cox regression analyses of clinicopathological characteristics and CLEVER-1$^+$TAM infiltration in the Zhongshan cohort. ACRG, Asian Cancer Research Group; CIN, chromosomal instability; CLEVER-1, common lymphatic endothelial and vascular endothelial receptor 1; GS, genomic stability; IFN, interferon; MSI, microsatellite instability; MSS, microsatellite stable; OS, overall survival; TAM, tumor-associated macrophage; TCGA, The Cancer Genome Atlas; ZSFC, Zhongshan Flow Cytometry.

p<0.05). These findings indicate that higher infiltration of CLEVER-1$^+$TAMs is associated with more advanced disease stages and may serve as a potential biomarker for disease progression.

Given these observations, we further examined the relationship between CLEVER-1$^+$TAMs and the TME, particularly in relation to histological and molecular subtypes. In addition to the traditional Laurén classification, The Cancer Genome Atlas (TCGA) and Asian Cancer Research Group (ACRG) subtyping provide molecular subtyping frameworks for GC. Interestingly, no significant differences were observed in CLEVER-1$^+$TAM infiltration among Laurén subtypes (online supplemental figure 2B). However, infiltration levels varied significantly across TCGA subtypes, with the highest levels observed in the genomically stable (GS) subtype (p<0.001; figure 4B). Similarly, in ACRG subtypes, CLEVER-1$^+$TAM infiltration was significantly higher in the microsatellite stable/epithelial-mesenchymal transition (EMT) group compared with other subtypes (p<0.001; figure 4C). Together, these results suggested that CLEVER-1$^+$TAMs are enriched in molecular subtypes associated with poor prognosis, suggesting their potential role in identifying aggressive GC phenotypes.

Survival analysis further demonstrated a clear association between high CLEVER-1$^+$TAM infiltration and poor OS in patients with GC. Kaplan-Meier survival curves revealed that high CLEVER-1$^+$TAM infiltration had significantly worse OS, particularly in stage II (log-rank test, p=0.029, HR=4.706; figure 4E) and stage III GC (log-rank test, p=0.011, HR=2.827; figure 4F). No significant difference was observed in stage I GC (log-rank test, p=0.719, HR=1.653; figure 4D), while the overall Zhongshan Cohort showed a strong association (log-rank test, p<0.001, HR=3.906; figure 4G). Furthermore, multivariate Cox regression analysis confirmed that high CLEVER-1$^+$TAM infiltration was an independent prognostic factor for poor OS (HR=3.433, 95% CI=1.677 to 7.027, p<0.001; figure 4H). Collectively, these findings highlight CLEVER-1$^+$TAMs as both a marker of disease progression and an independent predictor of adverse prognosis in GC.

Molecular and immunophenotypic characterization of CLEVER-1$^+$TAMs in GC

Building on the previous scRNA-seq analysis of macrophages in GC, we further classified them into CLEVER-1-positive (*STAB1*$^+$) and CLEVER-1-negative (*STAB1*$^-$) subpopulations to explore their distinct gene expression profiles. DEGs between *STAB1*$^+$ and *STAB1*$^-$ TAMs were identified from 26 primary GC tissue samples (GSE183904 data set). As shown in the volcano plot (figure 5A), *STAB1*$^+$ TAMs exhibited significant upregulation of genes associated with immune regulation and phagocytosis, such as *CD163*, *MRC1*, and *TGFBI*, while downregulating genes linked to pro-inflammatory responses, including *IL1RN* and *CCL20*.

To better understand the functional traits of *STAB1*$^+$ TAMs, we performed the Kyoto Encyclopedia of Genes and Genomes (KEGG) pathway and the GO enrichment analyses. KEGG analysis indicated that *STAB1*$^+$ TAMs were predominantly involved in the phagosome, lysosome, and cytokine–cytokine receptor interaction, underscoring their potential immunomodulatory roles (figure 5B). GO analysis further demonstrated their involvement in immune regulation, cell adhesion, and extracellular matrix organization, showcasing their diverse functional properties (figure 5C).

Given these findings, we analyzed the expression of M1 and M2-associated genes in *STAB1*$^+$ and *STAB1*$^-$ TAMs (figure 5D). *STAB1*$^+$TAMs exhibited a mixed immunophenotype, co-expressing both M1 markers (eg, *HLA-DPA1*, *HLA-DPB1*) and M2 markers (eg, *CD163* and *MRC1*). To validate these transcriptomic findings, we performed FCM on 23 fresh GC samples, confirming significantly higher levels of M2-like markers in CLEVER-1$^+$TAMs, including CD163 (p<0.01; figure 5E), CD206 (p<0.05; figure 5F), arginase-1 (Arg-1) (p<0.01; online supplemental figure 3A), transforming growth factor (TGF)-β (p<0.01; online supplemental figure 3B) and IL-10 (p<0.01; online supplemental figure 3C). Interestingly, CLEVER-1$^+$TAMs demonstrated a significant increase in human leukocyte antigen (HLA)-DR expression (p<0.01; figure 5G) and a noticeable trend towards elevated TNF-α expression (p=0.078; figure 5H), indicating a potential association despite the lack of statistical significance for TNF-α.

FCM data further corroborated transcriptomic findings, reinforcing the limitations of the conventional M1/M2 macrophage model. Notably, STAB1$^+$TAMs exhibited increased expression of both *CXCL9* and *SPP1* (figure 5D). Recent studies have proposed that the *CXCL9/SPP1* ratio, referred to as the "polarity" of TAMs, offers a more refined and clinically relevant metric than conventional M1/M2 markers.[30] To evaluate this, we assessed CXCL9 and osteopontin (OPN/SPP1) levels via FCM. OPN expression was significantly higher in CLEVER-1$^+$TAMs (p<0.01; online supplemental figure 4A), while CXCL9 levels were similar between the two groups (online supplemental figure 4B). A paired comparison of the CXCL9/OPN ratio between CLEVER-1$^+$ and CLEVER-1$^-$ TAMs revealed a statistically significant difference (p<0.05; online supplemental figure 4B), further supporting the notion that CLEVER-1$^+$ TAMs exhibit a polarity indicative of an immunosuppressive phenotype.

To assess immunophenotypic shifts across disease stages, we analyzed CLEVER-1$^+$ and CLEVER-1$^-$ TAMs at different TNM stages. M2-associated markers (TGF-β, IL-10, and Arg-1) progressively increased in advanced stages, suggesting a transition towards an immunosuppressive phenotype (figure 5; online supplemental figure 3D–H). In contrast, HLA-DR and TNF-α were significantly upregulated in earlier stages (figure 5; online supplemental figure 3I,J), implying that CLEVER-1$^+$TAMs initially exhibit a more activated or mixed phenotype before transitioning to immunosuppression. Conclusively, this stage-stratified approach reinforces our conclusion that CLEVER-1 expression may reflect a time-dependent

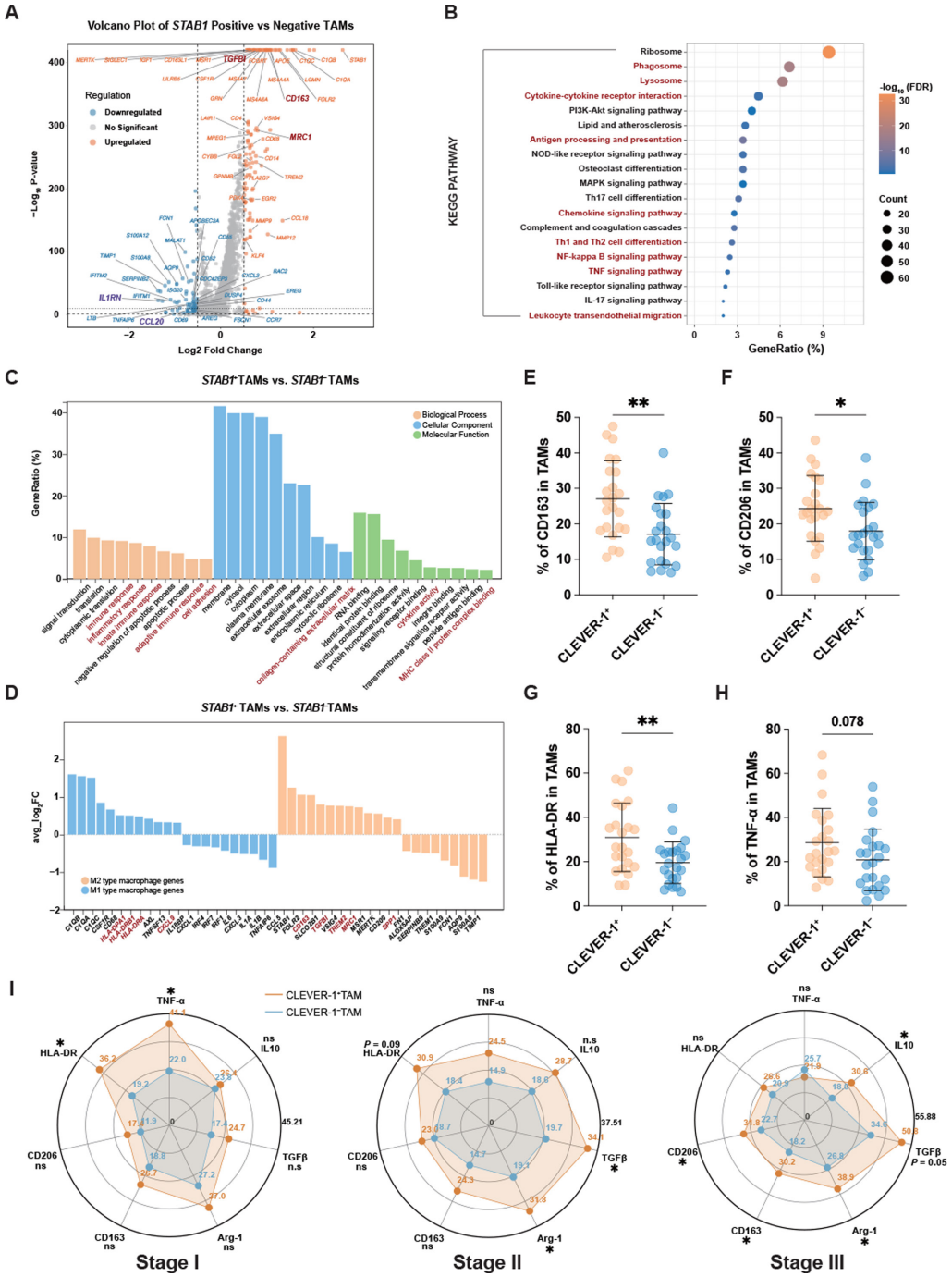

Figure 5 Differential gene expression and functional analysis of CLEVER-1-positive (*STAB1*$^+$) versus CLEVER-1-negative (*STAB1*$^-$) TAMs in GC. (A) Volcano plot illustrating the DEGs between *STAB1*$^+$ and *STAB1*$^-$TAMs in GC using single-cell RNA sequencing (n=26). Genes significantly upregulated (orange) and downregulated (blue) in *STAB1*$^+$TAMs are indicated (p<0.05, |$\log_2$ fold change|>1). (B) KEGG pathway enrichment analysis of DEGs between *STAB1*$^+$ and *STAB1*$^-$TAMs, revealing functional differences between these two populations. (C) GO enrichment analysis of DEGs between *STAB1*$^+$TAMs and *STAB1*$^-$TAMs highlighting key biological processes, cellular components, and molecular functions. (D) Bar plot showing the differential expression of M1-associated and M2-associated genes in *STAB1*$^+$TAMs compared with STAB1$^-$TAMs. (E–H) FCM analysis of 23 fresh GC samples showing the expression of M2-like markers CD163 (E), CD206 (F), and M1-like markers HLA-DR (G), TNF-α (H) expression on CLEVER-1$^+$ and CLEVER-1$^-$ TAMs. Statistical analysis by two-tailed unpaired t-test. Small horizontal lines indicate the mean (±SD). *p<0.05, **p<0.01 and ***p<0.001. (I) Radar plots illustrating the expression profiles of CLEVER-1$^+$ and CLEVER-1$^-$ TAMs markers (HLA-DR, TNF-α, IL-10, TGF-β, Arg-1, CD163, and CD206), stratified by tumor, node, metastases stages. Statistical analysis by two-tailed unpaired t-test and two-tailed unpaired Mann-Whitney U test. *p<0.05; n.s, not significant. Arg-1, arginase-1; DEG, differentially expressed gene; FDR, false discovery rate; GC, gastric cancer; GO, Gene Ontology; HLA-DR, human leukocyte antigen-DR; IL-10, interleukin-10; KEGG, Kyoto Encyclopedia of Genes and Genomes; MACS, magnetic-activated cell sorting; PDGC, Percoll density gradient centrifugation; TAM, tumor-associated macrophage; TGF-β, transforming growth factor-β; TNF-α, tumor necrosis factor-α.

polarization of TAMs, transitioning from immunoactivating to immunosuppressive states. Overall, these findings support the notion that CLEVER-1$^+$TAMs constitute an immunologically dynamic subset, exhibiting both M1 and M2-like properties of macrophages and contributing to the complexity of the GC immune landscape.

CLEVER-1$^+$TAMs are associated with tumor infiltration CD8$^+$T cell dysfunction in GC

Building on the previous findings, CLEVER-1$^+$TAMs exhibited significant enrichment in multiple T cell-related regulatory pathways, including cytokine–cytokine receptor interaction, NF-kappa B signaling, Th1/Th2 cell differentiation, and MAPK signaling (figure 5B). These observations suggest that CLEVER-1$^+$TAMs may modulate CD8$^+$T cell activity, thereby influencing clinical prognosis.

To explore this potential relationship, we delved deeper into the correlation between CLEVER-1$^+$TAM infiltration and CD8$^+$T cell function in GC. In the ZSFC cohort, 60 patients undergoing radical gastrectomy were included in a functional assessment of tumor-infiltrating CD8$^+$T cells. Kaplan-Meier survival curves revealed that high CLEVER-1$^+$TAM infiltration was significantly associated with poorer OS (log-rank test, p=0.024, HR=2.253; figure 6A) and DFS (log-rank test, p=0.025, HR=2.314; figure 6B), highlighting its adverse prognostic impact.

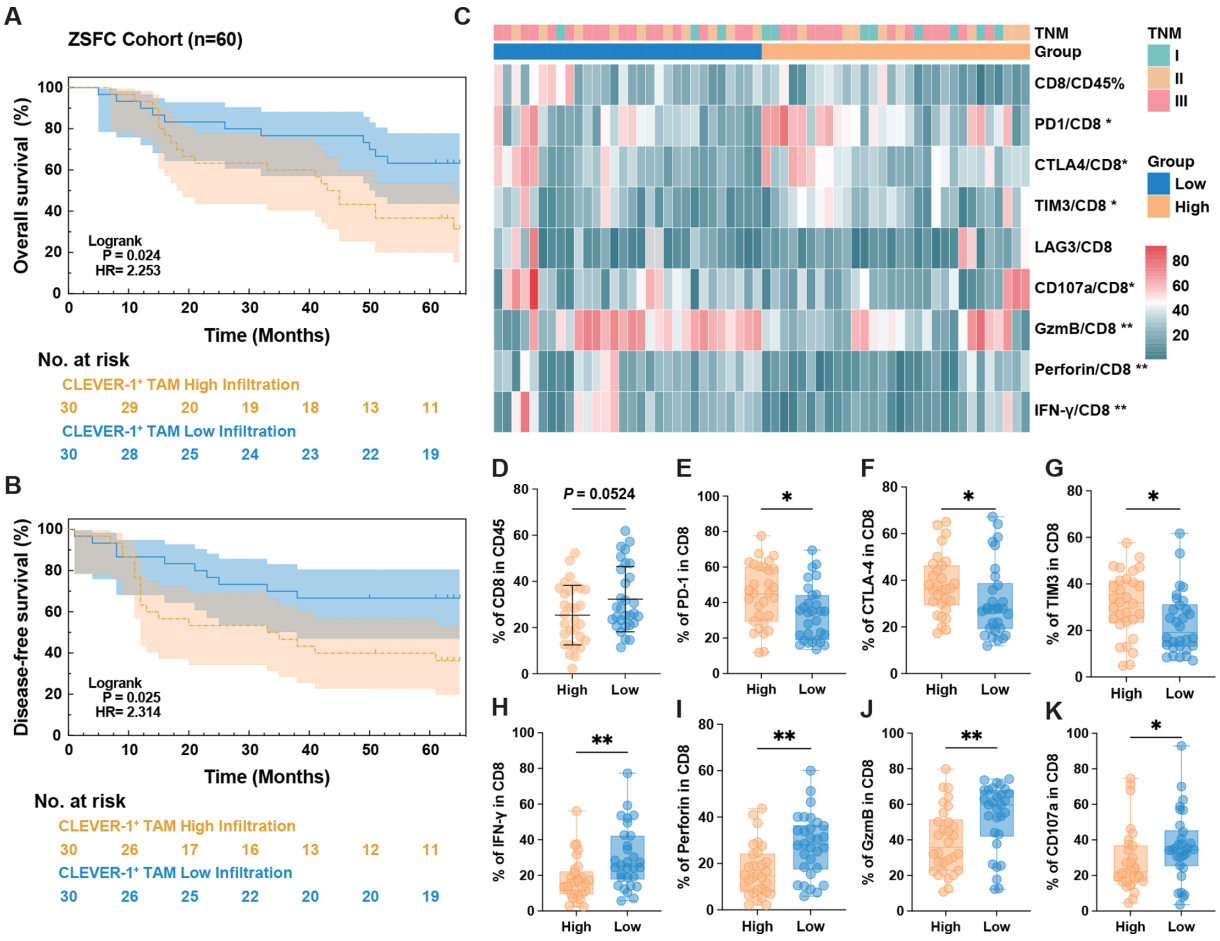

Figure 6 Effect of CLEVER-1$^+$ TAM infiltration on CD8$^+$ T-cell antitumor activity and survival outcomes in patients with GC. (A–B) Kaplan-Meier survival curves for OS (A) and DFS (B), stratified by CLEVER-1$^+$TAM infiltration levels in patients with GC from the ZSFC cohort (n=60). Statistical analysis was performed using the log-rank test, and survival probabilities are shown as 95% CIs. (C) Heatmap illustrating the expression of CD8$^+$T cell effector molecules and immune checkpoint relative to CLEVER-1$^+$TAM infiltration levels, based on flow cytometry analysis (Z-score normalization). Statistical significance was determined using the two-tailed unpaired Mann-Whitney U test. *p<0.05, **p<0.01, and ***p<0.001. (D) Quantification of tumor-infiltrating CD8$^+$T cells among patient with high and low CLEVER-1$^+$TAM infiltration GC subgroups. Statistical analysis by two-tailed unpaired t-test. Small horizontal lines indicate the mean (±SD) (p=0.0524). (E–F) Quantification of exhausted markers (PD-1 (E), CTLA-4 (F), and TIM-3 (G)) and effector cytokines (IFN-γ (H), perforin (I), GZMB (J), and CD107a (K)) expression on CD8$^+$T cells among patient with high and low CLEVER-1$^+$TAM infiltration GC subgroups. Statistical analysis by two-tailed unpaired Mann-Whitney U test. Box shows the median (±IQR), and whiskers indicate min-max values. *p<0.05, **p<0.01, ***p<0.001. CTLA4, cytotoxic T-lymphocyte antigen 4; DFS, disease-free survival; GC, gastric cancer; GzmB, granzyme B; IFN-γ, interferon-gamma; IHC, immunohistochemistry; LAG3, lymphocyte-activation gene 3; PD-1, programmed cell death protein 1; TAM, tumor-associated macrophage; TIM-3, T-cell immunoglobulin and mucin-domain containing-3; ZSFC, Zhongshan Flow Cytometry.

Subsequently, we investigated how CLEVER-1$^+$TAMs influence CD8$^+$T cell function by profiling the expression of key effector and immune checkpoint molecules. The heatmap provides an overview of CD8$^+$T cell characteristics in relation to CLEVER-1$^+$ TAM abundance (figure 6C). Quantification of tumor-infiltrating CD8$^+$T cells demonstrated a trend towards lower infiltration in patients with high CLEVER-1$^+$TAMs, though this difference was not statistically significant (unpaired t-tests, p=0.0524; figure 6D). Validation in the Zhongshan Cohort confirmed significantly lower CD8$^+$T cell infiltration in patients with high CLEVER-1$^+$ TAM levels (p=0.03; online supplemental figure 2C).

Further analysis showed significant upregulation of exhaustion markers in CD8$^+$ T cells in the high CLEVER-1$^+$ TAM group, with increased levels of PD-1 (p=0.01; figure 6E), cytotoxic T-lymphocyte antigen-4 (p=0.02; figure 6F), and T-cell immunoglobulin and mucin-domain containing-3 (p=0.02; figure 6G). Conversely, effector cytokine expression was markedly reduced, with lower levels of interferon (IFN)-γ (p<0.01; figure 6H), perforin (p<0.01; figure 6), granzyme B (GzmB) (p<0.01; figure 6J), and CD107a (p=0.04; figure 6K). These findings suggest that elevated CLEVER-1$^+$TAM infiltration contributes to poorer clinical outcomes in patients with GC by promoting an exhausted state of CD8$^+$ T cells and driving immunosuppression within the TME.

Collectively, these results highlight a theoretical basis for understanding the immunosuppressive microenvironment,[31] poor prognosis,[32] and increased immunotherapy resistance[33] in GC.

Blockade of CLEVER-1 reprograms TAMs toward an immunostimulatory state in GC

As the experimental design (figure 1A) outlined, single-cell suspensions were obtained from eight fresh GC samples and exposed to CLEVER-1 blockade or isotype. CD14$^+$TAMs were then isolated via magnetic bead sorting and subjected to smart-seq2 for transcriptomic analysis.

After the CLEVER-1 blockade, DEGs from treated TAMs were identified by comparison with controls. The heatmap demonstrated clear alterations in gene expression profiles (figure 1B), indicating significant transcriptional reprogramming of TAMs. GO enrichment analysis revealed activation of immune-related biological processes, notably inflammatory response, and enhanced production of TNF, IL-1β, and IFN-γ, as well as increased T-cell proliferation and migration (figure 5C,D). Cellular component analysis indicated marked enrichment in antigen presentation-associated compartments, including the plasma membrane and extracellular exosomes. Molecular function analysis highlighted the upregulation of receptor-mediated signaling, cytokine binding, and integrin interactions, collectively supporting the notion of enhanced antigen presentation and immune activation following anti-CLEVER-1 treatment.

Pathway analysis further corroborated the pro-inflammatory reprogramming of TAMs after treatment. KEGG pathway enrichment revealed significant activation of pathways involved in cytokine signaling, innate immune sensing (eg, toll-like and NOD-like receptor pathways), inflammatory signal transduction (eg, NF-κB and JAK-STAT pathways), chemokine signaling, T-cell receptor signaling, and immune checkpoint regulation (programmed death-ligand 1/programmed death-1 [PD-L1/PD-1] pathway) (figure 1E).

To further characterize these changes, the expression of key immune-regulatory molecules was also examined. TAMs treated with CLEVER-1 blockade exhibited increased expression of genes encoding pro-inflammatory chemokines (eg, *CXCL9*, *CXCL10*), cytokines (eg, *TNF*, *IL-1B*), and co-stimulatory receptors (eg, *CD80*, *CD86*); whereas anti-inflammatory markers and metabolic-related genes (eg, *ARG1*, *IL-10*, *PPARG*) were downregulated (figure 1F).

FCM further validated the upregulation of immunostimulatory markers identified in the transcriptomic analysis and associated with immune pathways enriched in GO and KEGG analyses. CLEVER-1 blockade significantly increased the proportion of TAMs expressing CXCL9 (p=0.03; figure 1G, left panel), along with elevated co-stimulatory receptors CD80 (p=0.02; figure 1G, middle panel) and CD86 (p=0.03, figure 1G, right panel). Other markers, including HLA-DR, OPN/SPP1, and CD206, exhibited no statistically significant differences (online supplemental figure E–G). These results further support that CLEVER-1 inhibition reprograms TAMs toward an immunostimulatory phenotype characterized by enhanced antigen presentation and T-cell activation.

Dynamic CLEVER-1$^+$TAM infiltration predicts response and mediates adaptive resistance to anti-PD-1-based immunochemotherapy in GC

Given the critical role observed for CLEVER-1$^+$TAMs in shaping the immunosuppressive TME of GC, we examined their infiltration in paired tumor tissues from 12 patients with GC before and after four cycles of anti-PD-1-based neoadjuvant immunochemotherapy (SOX+anti-PD-1) (online supplemental figure 5A,B). Baseline CLEVER-1$^+$TAM infiltration was significantly lower in responders compared with non-responders (p<0.01, figure 2A). However, this difference was abolished in post-treatment residual tumor tissues of responders and non-responders (online supplemental figure 5C), suggesting that the surviving tumor niches may undergo immune adaptation, leading to a similar immunosuppressive microenvironment. Interestingly, there was a trend toward increased CLEVER-1$^+$TAM infiltration following treatment compared with baseline (online supplemental figure 5E), with a significant increase observed specifically in responders (p<0.01, figure 2B). In contrast, non-responders maintained persistently high levels of CLEVER-1$^+$TAM infiltration throughout therapy (online supplemental figure 5F,G).

This phenomenon suggests that while a lower baseline CLEVER-1$^+$TAM infiltration may predict a better

response to immunotherapy, the treatment itself may drive an accumulation of CLEVER-1$^+$TAM in the TME. This suggests that immunotherapy-induced changes in CLEVER-1$^+$TAM dynamics might play a role in remodeling the TME and affect treatment outcomes.

Targeting CLEVER-1 serves as a potential combinatorial strategy to overcome adaptive resistance to PD-1 inhibitor-based therapy through resolving CD8$^+$ T-cell hyporesponsiveness in GC

To investigate whether CLEVER-1-targeted TAMs modulation enhances CD8$^+$T cell activation via paracrine signaling, we performed co-culture experiments using CD8$^+$ T cells and TAMs pretreated with either anti-CLEVER-1 or IgG_4 control, alongside CD8$^+$ T cells cultured alone as a reference (online supplemental figure 6A). FCM analysis revealed that TAMs significantly increased CD8$^+$T cell apoptosis, which was mitigated by CLEVER-1 blockade (figure 2C; online supplemental figure 6H). Similarly, TAMs suppressed CD8$^+$T cell proliferation, as indicated by reduced Ki-67 expression, whereas CLEVER-1 blockade reversed their proliferative capacity (figure 2D; online supplemental figure 6I). CLEVER-1 inhibition rescued TAM-suppressed perforin expression in CD8$^+$T cells (figure 2E; online supplemental figure 6J), whereas IFN-γ and GzmB exhibited a non-significant trend toward recovery (online supplemental figure 6K,L), suggesting a partial reversal of TAM-mediated suppression. These findings demonstrate that CLEVER-1$^+$TAMs suppress CD8$^+$T cell activation through direct secretion and that CLEVER-1 blockade restores CD8$^+$T cell function by alleviating TAM-mediated immunosuppression.

To further assess its clinical translational potential, single-cell suspensions from fresh GC samples were treated with CLEVER-1 blockade, nivolumab, and their combination, following the experimental set-up (figure 2F). FCM analysis demonstrated that CLEVER-1 blockade, alone or in combination with nivolumab, significantly enhanced the expression of effector molecules in CD8$^+$T cells, including GzmB, IFN-γ, and perforin (figure 2G–I). Notably, the combination treatment induced the highest levels of these markers, suggesting a potential synergistic effect in promoting CD8$^+$T cell functionality.

Given previous findings that CLEVER-1$^+$TAM infiltration is associated with reduced responsiveness and adaptive resistance to anti-PD-1 immunotherapy (figure 6D,E; online supplemental figure 5), we further investigated the therapeutic potential of combination treatment in enhancing antitumor efficacy.

In CD45$^-$EpCAM$^+$ tumor cells, Annexin V staining demonstrated increased apoptosis following treatment, with the combination of CLEVER-1 blockade and nivolumab exerting the strongest pro-apoptotic effect (figure 6J,K). To define the role of CLEVER-1$^+$TAMs in this response, we stratified patients by CLEVER-1$^+$TAM infiltration levels. In tumors with high CLEVER-1$^+$TAM infiltration, CLEVER-1 blockade significantly enhanced tumor cell apoptosis, with a marked synergistic effect when combined with nivolumab (figure 2J). In contrast, in tumors with low CLEVER-1$^+$TAM infiltration, CLEVER-1 blockade had a weaker sensitizing effect on nivolumab, suggesting that CLEVER-1$^+$TAM abundance influences the responsiveness to combination immunotherapy and may serve as a predictive biomarker for immunotherapy efficacy.

As high CLEVER-1$^+$TAM infiltration correlates with poor prognosis, immunotherapy resistance, and increased accumulation in residual tumors following treatment, anti-CLEVER-1 treatment emerges as a promising strategy to overcome anti-PD-1 resistance by reprogramming TAMs to relieve immunosuppression, restore CD8$^+$T cell functionality, and enhance tumor cell apoptosis, with a synergistic effect when combined with PD-1 inhibition.

DISCUSSION

The Food and Drug Administration approval of immune checkpoint inhibitors has ushered in a new era of immunotherapy for GC.[34 35] Although patients with microsatellite instability and Epstein-Barr virus-associated GC generally exhibit favorable responses, the majority—particularly those with immune "cold" subtypes such as GS and EMT, show limited benefit.[36 37] While combined positive score scoring and tumor mutational burden provide some guidance for selecting patients for immunotherapy,[38–40] an optimal predictive biomarker remains elusive. Given their key role in shaping the tumor immune landscape, TAMs have gained attention as potential immunotherapy response markers.[18 41] Targeting TAMs may offer a promising approach to enhancing immunotherapy sensitivity.[18]

CLEVER-1 has emerged as a marker of an immunosuppressive TAM subset, whose functional blockade with bexmarilimab (an anti-CLEVER-1 antibody[42]) restores antitumor immunity.[26 43] In the first-in-human Phase I/II MATINS trial (NCT03733990), patients with GC achieved a 33% disease control rate, ranking third among solid tumors.[43] However, the mechanism and therapeutic implications of CLEVER-1 blockade in GC remain unclear. Here, we confirmed that CLEVER-1 is predominantly expressed on TAMs in GC and correlates with poor prognosis, providing supporting evidence in this context.[23 24 44] Notably, our data revealed that the CLEVER-1$^+$TAM infiltration increased with tumor progression, and its association with adverse outcomes becomes more pronounced in advanced disease. Single-cell analysis demonstrated that CLEVER-1$^+$TAMs co-express both M1 and M2 markers, while FCM further confirmed their dynamic immunophenotype. These findings suggest that CLEVER-1$^+$TAMs may initially retain some antitumor potential but progressively transition into an immunosuppressive state as the tumor evolves, which could explain previous conflicting prognostic of CLEVER-1$^+$TAM associations across cancer types.[45–47]

Importantly, we found that patients with high baseline CLEVER-1$^+$TAM infiltration exhibited a lower response to anti-PD-1 therapy. Moreover, in responders,

CLEVER-1$^+$TAM infiltration frequently increased following treatment, suggesting a role in adaptive resistance to immunotherapy. Unlike prior studies focusing on the response versus non-response to anti-CLEVER-1 therapy, our study is the first to emphasize the impact of CLEVER-1$^+$TAM infiltration on the immunochemotherapy response in GC. The MATINS trial found that higher intratumoral CLEVER-1$^+$TAM levels were associated with disease control after bexmarilimab treatment.[43] Our study extends these observations by demonstrating that CLEVER-1 blockade not only reprograms TAMs but also enhances the efficacy of anti-PD-1 therapy, particularly in tumors with high CLEVER-1$^+$TAM infiltration. These findings suggest that CLEVER-1$^+$TAM abundance may serve as a predictive biomarker for response to combination immunotherapy, supporting the rationale for targeting CLEVER-1 to overcome TAM-driven resistance to PD-1 blockade.

Mechanistically, bexmarilimab has been shown to enhance CD8$^+$T cell proliferation by suppressing TAM-mediated lysosomal acidification and antigen cross-presentation via LXR/RXR-PPAR pathway inhibition.[26] Extending these findings to GC, we demonstrate that anti-CLEVER-1 reprograms TAMs via downregulation of *PPARG, ARG1, IL10* (disrupting lipid-driven immunosuppression) while concurrent upregulation of pro-inflammatory mediators (*TNF, IL1B, IFNG*), chemotactic signals (*CXCL9, CXCL10*), and co-stimulation markers (CD80, CD86). This conserved immunostimulatory axis is further evidenced by bexmarilimab-induced CXCL10 secretion and CD8$^+$T cell activation in ovarian TAMs.[48] Importantly, bexmarilimab-induced peripheral T-cell activation[26] mechanistically complements our observation of enhanced intratumoral CD8$^+$T cell effector functions following treatment, providing convergent evidence that CLEVER-1 blockade orchestrates anti-tumor immunity through both localized and systemic axes.

This study has several limitations. First, the lack of an in vivo immune-competent GC mouse model prevented us from performing functional validation in a preclinical setting. Future studies could employ patient-derived xenografts with humanized immune systems to further investigate CLEVER-1 blockade in vivo. Second, our sample size for immunochemotherapy was limited, and selection bias may exist since patients with the poorest outcomes—those who remain unresectable after immunochemotherapy—were difficult to include. Third, our study lacks an in-depth exploration of the long-term effects of CLEVER-1 blockade on the TME. Additionally, a more detailed mechanistic investigation, particularly regarding downstream signaling pathways involved in CLEVER-1-mediated immune modulation, is warranted. Furthermore, our findings were validated in only two independent cohorts, which may limit their generalizability. Therefore, future research using larger, more diverse, and multi-institutional patient populations, along with longitudinal studies, is recommended to fully assess the therapeutic potential, safety profile, and validation of targeting CLEVER-1 in GC.

Acknowledgements The authors thank Professor Yihong Sun, Professor Kuntang Shen and Professor Xuefei Wang (Gastric Cancer Center, Zhongshan Hospital, Fudan University, Shanghai, China) for their invaluable suggestions and assistance with specimen collection. The authors thank Professor Yingyong Hou (Department of Pathology, Zhongshan Hospital, Fudan University, Shanghai, China) for their excellent pathological technology support. The authors acknowledge BioRender (BioRender.com) for providing the tools to create Schematics. We would like to express our gratitude to all individuals who provided valuable support during this study. On a personal note, I (KY) am deeply grateful to my grandmother for her unwavering support and motivation, which have been a source of strength during the preparation of this manuscript. Additionally, I would like to sincerely thank Ms Yudi Zhao (School of Public Health, Imperial College London) for her encouragement throughout this project.

Contributors KY was responsible for conducting the research, acquiring and analyzing data, performing statistical analysis, interpreting the results, and drafting the manuscript. YC guided the research and revised the figures and manuscript. ZZ provided research samples and maintained the research cohort. LW, YG, and TX provided technical and material support. XZ and XG conducted pathological research and analysis. JQ and ZS proposed the research concepts, designed the study, and reviewed and proofread the manuscript. All authors read and approved the final manuscript. JQ was responsible for the overall content as the guarantor. The manuscript has been edited with the assistance of Grammarly and ChatGPT to enhance the clarity and quality of the language.

Funding This study was funded by grants from the National Natural Science Foundation of China (82172694, 82373256, 82372792).

Competing interests None declared.

Patient consent for publication Not applicable.

Ethics approval This study was approved by the Ethics Committee of Zhongshan Hospital, Fudan University (No. B2024-261). Participants gave informed consent to participate in the study before taking part.

Provenance and peer review Not commissioned; externally peer reviewed.

Data availability statement Data are available upon reasonable request.

ORCID iDs
Kuan Yu http://orcid.org/0000-0001-6272-9612
Jing Qin http://orcid.org/0000-0001-8833-3165

REFERENCES

1 Arnold M, Park JY, Camargo MC, *et al*. Is gastric cancer becoming a rare disease? A global assessment of predicted incidence trends to 2035. *Gut* 2020;69:823–9.
2 Lin Y, Zheng Y, Wang H-L, *et al*. Global Patterns and Trends in Gastric Cancer Incidence Rates (1988-2012) and Predictions to 2030. *Gastroenterology* 2021;161:116–27.
3 Bray F, Laversanne M, Sung H, *et al*. Global cancer statistics 2022: GLOBOCAN estimates of incidence and mortality worldwide for 36 cancers in 185 countries. *CA Cancer J Clin* 2024;74:229–63.
4 Smyth EC, Nilsson M, Grabsch HI, *et al*. Gastric cancer. *Lancet* 2020;396:635–48.

5 Alsina M, Arrazubi V, Diez M, *et al*. Current developments in gastric cancer: from molecular profiling to treatment strategy. *Nat Rev Gastroenterol Hepatol* 2023;20:155–70.
6 Morgan E, Arnold M, Camargo MC, *et al*. The current and future incidence and mortality of gastric cancer in 185 countries, 2020-40: A population-based modelling study. *EClinicalMedicine* 2022;47:101404.
7 Li K, Zhang A, Li X, *et al*. Advances in clinical immunotherapy for gastric cancer. *Biochim Biophys Acta Rev Cancer* 2021;1876:188615.
8 Lordick F, Carneiro F, Cascinu S, *et al*. Gastric cancer: ESMO Clinical Practice Guideline for diagnosis, treatment and follow-up. *Ann Oncol* 2022;33:1005–20.
9 Oliveira G, Wu CJ. Dynamics and specificities of T cells in cancer immunotherapy. *Nat Rev Cancer* 2023;23:295–316.
10 Zhang Y, Zhang Z. The history and advances in cancer immunotherapy: understanding the characteristics of tumor-infiltrating immune cells and their therapeutic implications. *Cell Mol Immunol* 2020;17:807–21.
11 Tang T, Huang X, Zhang G, *et al*. Advantages of targeting the tumor immune microenvironment over blocking immune checkpoint in cancer immunotherapy. *Signal Transduct Target Ther* 2021;6:72.
12 Dvorak HF. Tumors: wounds that do not heal-redux. *Cancer Immunol Res* 2015;3:1–11.
13 Wang Y, Johnson KCC, Gatti-Mays ME, *et al*. Emerging strategies in targeting tumor-resident myeloid cells for cancer immunotherapy. *J Hematol Oncol* 2022;15:118.
14 Cassetta L, Pollard JW. A timeline of tumour-associated macrophage biology. *Nat Rev Cancer* 2023;23:238–57.
15 Sica A, Mantovani A. Macrophage plasticity and polarization: in vivo veritas. *J Clin Invest* 2012;122:787–95.
16 Lv K, Sun M, Fang H, *et al*. Targeting myeloid checkpoint Siglec-10 reactivates antitumor immunity and improves anti-programmed cell death 1 efficacy in gastric cancer. *J Immunother Cancer* 2023;11:e007669.
17 Cao Y, Yu K, Zhang Z, *et al*. Blockade of V-domain immunoglobulin suppressor of T-cell activation reprograms tumour-associated macrophages and improves efficacy of PD-1 inhibitor in gastric cancer. *Clin Transl Med* 2024;14:e1578.
18 Gambardella V, Castillo J, Tarazona N, *et al*. The role of tumor-associated macrophages in gastric cancer development and their potential as a therapeutic target. *Cancer Treat Rev* 2020;86:102015.
19 Irjala H, Elima K, Johansson E-L, *et al*. The same endothelial receptor controls lymphocyte traffic both in vascular and lymphatic vessels. *Eur J Immunol* 2003;33:815–24.
20 Palani S, Maksimow M, Miiluniemi M, *et al*. Stabilin-1/CLEVER-1, a type 2 macrophage marker, is an adhesion and scavenging molecule on human placental macrophages. *Eur J Immunol* 2011;41:2052–63.
21 Kzhyshkowska J, Gratchev A, Goerdt S. Stabilin-1, a homeostatic scavenger receptor with multiple functions. *J Cell Mol Med* 2006;10:635–49.
22 Salmi M, Koskinen K, Henttinen T, *et al*. CLEVER-1 mediates lymphocyte transmigration through vascular and lymphatic endothelium. *Blood* 2004;104:3849–57.
23 Karikoski M, Marttila-Ichihara F, Elima K, *et al*. Clever-1/stabilin-1 controls cancer growth and metastasis. *Clin Cancer Res* 2014;20:6452–64.
24 Viitala M, Virtakoivu R, Tadayon S, *et al*. Immunotherapeutic Blockade of Macrophage Clever-1 Reactivates the $CD8^+$ T-cell Response against Immunosuppressive Tumors. *Clin Cancer Res* 2019;25:3289–303.
25 Hollmén M, Figueiredo CR, Jalkanen S. New tools to prevent cancer growth and spread: a “Clever” approach. *Br J Cancer* 2020;123:501–9.
26 Virtakoivu R, Rannikko JH, Viitala M, *et al*. Systemic Blockade of Clever-1 Elicits Lymphocyte Activation Alongside Checkpoint Molecule Downregulation in Patients with Solid Tumors: Results from a Phase I/II Clinical Trial. *Clin Cancer Res* 2021;27:4205–20.
27 Information NCfB. GEO dataset GSE183904. 2021. Available: https://www.ncbi.nlm.nih.gov/geo/query/acc.cgi?acc=GSE183904 [Accessed 12 Nov 2023].
28 Kumar V, Ramnarayanan K, Sundar R, *et al*. Single-Cell Atlas of Lineage States, Tumor Microenvironment, and Subtype-Specific Expression Programs in Gastric Cancer. *Cancer Discov* 2022;12:670–91.
29 Japanese Gastric Cancer Association. Japanese classification of gastric carcinoma: 3rd English edition. *Gastric Cancer* 2011;14:101–12.
30 Bill R, Wirapati P, Messemaker M, *et al*. *CXCL9:SPP1* macrophage polarity identifies a network of cellular programs that control human cancers. *Science* 2023;381:515–24.
31 Cao LL, Lu H, Soutto M, *et al*. Multivalent tyrosine kinase inhibition promotes T cell recruitment to immune-desert gastric cancers by restricting epithelial-mesenchymal transition via tumour-intrinsic IFN-γ signalling. *Gut* 2023;72:2038–50.
32 Yu K, Gu Y, Zhang P, *et al*. Intratumoral PD-1^+CD8^+ T cells associate poor clinical outcomes and adjuvant chemotherapeutic benefit in gastric cancer. *Br J Cancer* 2022;127:1709–17.
33 Dong D, Yu X, Xu J, *et al*. Cellular and molecular mechanisms of gastrointestinal cancer liver metastases and drug resistance. *Drug Resist Updat* 2024;77:101125.
34 Administration USFaD. FDA approves nivolumab in combination with chemotherapy for metastatic gastric cancer and esophageal adenocarcinoma. 2021. Available: https://www.fda.gov/drugs/resources-information-approved-drugs/fda-approves-nivolumab-combination-chemotherapy-metastatic-gastric-cancer-and-esophageal [Accessed 07 Nov 2024].
35 Administration USFaD. FDA approves pembrolizumab for esophageal or GEJ carcinoma. 2021. Available: https://www.fda.gov/drugs/resources-information-approved-drugs/fda-approves-pembrolizumab-esophageal-or-gej-carcinoma [Accessed 07 Nov 2024].
36 Shitara K, Ajani JA, Moehler M, *et al*. Nivolumab plus chemotherapy or ipilimumab in gastro-oesophageal cancer. *Nature New Biol* 2022;603:942–8.
37 Kim ST, Cristescu R, Bass AJ, *et al*. Comprehensive molecular characterization of clinical responses to PD-1 inhibition in metastatic gastric cancer. *Nat Med* 2018;24:1449–58.
38 Moutafi M, Rimm DL. Putting the Microenvironment into the Immunotherapy Companion Diagnostic. *Clin Cancer Res* 2021;27:3812–4.
39 Robert ME, Rüschoff J, Jasani B, *et al*. High Interobserver Variability Among Pathologists Using Combined Positive Score to Evaluate PD-L1 Expression in Gastric, Gastroesophageal Junction, and Esophageal Adenocarcinoma. *Mod Pathol* 2023;36:100154.
40 Lei M, Janjigian YY, Ajani JA, *et al*. Abstract CT023: Nivolumab (NIVO) plus chemotherapy (chemo) vs chemo as first-line (1L) treatment for advanced gastric cancer/gastroesophageal junction cancer/esophageal adenocarcinoma (GC/GEJC/EAC): CheckMate 649 biomarker analyses. *Cancer Res* 2022;82:CT023.
41 Carroll TM, Chadwick JA, Owen RP, *et al*. Tumor monocyte content predicts immunochemotherapy outcomes in esophageal adenocarcinoma. *Cancer Cell* 2023;41:1222–41.
42 Hollmén M, Maksimow M, Rannikko JH, *et al*. Nonclinical Characterization of Bexmarilimab, a Clever-1-Targeting Antibody for Supporting Immune Defense Against Cancers. *Mol Cancer Ther* 2022;21:1207–18.
43 Rannikko JH, Verlingue L, de Miguel M, *et al*. Bexmarilimab-induced macrophage activation leads to treatment benefit in solid tumors: The phase I/II first-in-human MATINS trial. *Cell Rep Med* 2023;4:101307.
44 Junttila A, Helminen O, Väyrynen JP, *et al*. Immunophenotype based on inflammatory cells, PD-1/PD-L1 signalling pathway and M2 macrophages predicts survival in gastric cancer. *Br J Cancer* 2020;123:1625–32.
45 Kwon M, Yeo SC, Lee JS, *et al*. Not CD68 but stabilin-1 expression is associated with the risk of recurrence in patients with oral cavity squamous cell carcinoma. *Head Neck* 2019;41:2058–64.
46 Algars A, Irjala H, Vaittinen S, *et al*. Type and location of tumor-infiltrating macrophages and lymphatic vessels predict survival of colorectal cancer patients. *Int J Cancer* 2012;131:864–73.
47 Mutka M, Virtakoivu R, Joensuu K, *et al*. Clever-1 positive macrophages in breast cancer. *Breast Cancer Res Treat* 2022;195:237–48.
48 Rannikko JH, Bono P, Hynninen J, *et al*. Bexmarilimab Activates Human Tumor-Associated Macrophages to Support Adaptive Immune Responses in Interferon-Poor Immune Microenvironments. *Cancer Immunol Res* 2024;12:48–59.